Na₃MnZr(PO₄)₃: A High-Voltage Cathode for Sodium Batteries
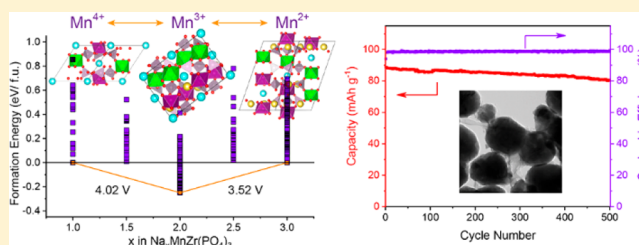
Hongcai Gao,[†,#] Ieuan D. Seymour,[‡,#] Sen Xin,[†] Leigang Xue,[†] Graeme Henkelman,[‡] and John B. Goodenough*,[†]

[†]Texas Materials Institute, The University of Texas at Austin, Austin, Texas 78712, United States
[‡]Department of Chemistry and the Institute for Computational Engineering and Sciences, The University of Texas at Austin, Austin, Texas 78712, United States

S Supporting Information

ABSTRACT: Sodium batteries have been regarded as promising candidates for large-scale energy storage application, provided cathode hosts with high energy density and long cycle life can be found. Herein, we report NASICON-structured Na₃MnZr(PO₄)₃ as a cathode for sodium batteries that exhibits an electrochemical performance superior to those of other manganese phosphate cathodes reported in the literature. Both the Mn^{4+}/Mn^{3+} and Mn^{3+}/Mn^{2+} redox couples are reversibly accessed in Na₃MnZr(PO₄)₃, providing high discharge voltage plateaus at 4.0 and 3.5 V, respectively. A high discharge capacity of 105 mAh g⁻¹ was obtained from Na₃MnZr(PO₄)₃ with a small variation of lattice parameters and a small volume change on extraction of two Na⁺ ions per formula unit. Moreover, Na₃MnZr(PO₄)₃ exhibits an excellent cycling stability, retaining 91% of the initial capacity after 500 charge/discharge cycles at 0.5 C rate. On the basis of structural analysis and density functional theory calculations, we have proposed a detailed desodiation pathway from Na₃MnZr(PO₄)₃ where Mn and Zr are disordered within the structure. We further show that the cooperative Jahn−Teller distortion of Mn^{3+} is suppressed in the cathode and that Na₂MnZr(PO₄)₃ is a stable phase.

INTRODUCTION

The integration of electric power generated from renewable sunlight and wind energy cannot be used unless it is stored in large-scale rechargeable batteries to smooth the supply of this electric power into the grid.[1,2] The ubiquitous availability of sodium from the oceans makes sodium batteries preferable to lithium batteries provided cathode hosts for Na⁺ extraction/insertion can be identified with sufficiently high voltage versus Na⁺/Na, a long cycle life, and fast charge/discharge rates.[3−5] The stored energy density is $<V(q)> \times Q(I_{dis})$ at a constant current $I_{dis} = dq/dt$, where $<V(q)>$ is the cell voltage averaged over the state of charge q and the capacity $Q(I_{dis})$ is the number of electrons transferred from the anode to the cathode per unit weight and/or volume in the time Δt for the electrochemical reaction at a desired rate between the two electrodes.[6] Because the electrodes change volume during a charge/discharge cycle, a small volume change of the cathodes during a charge/discharge cycle is preferred even with a liquid electrolyte.

A number of layered transition-metal oxides have been investigated as cathodes for a sodium battery, but they have been plagued by large volume changes and phase instabilities during cycling.[7−9] However, transition-metal cyanides with a Prussian-blue structure provide low-cost, facile synthesis and low activation energies for Na⁺ insertion/extraction.[10−14] Another important category of Na⁺ cathode hosts consists of polyanionic transition-metal compounds with open-framework

structures.[15−19] The strong binding in the polyanions can offer structural stability and a relatively small volume change during Na⁺ insertion/extraction over a large solid-solution range.[20,21] Recently, several manganese-based polyanionic compounds have been shown to exhibit an interestingly high voltage versus sodium,[22,23] but an unacceptable performance has been attributed to Jahn−Teller distortions of Mn^{3+} and/or a disproportionation reaction of surface Mn, $2Mn^{3+} = Mn^{2+} + Mn^{4+}$, with Mn^{2+} dissolution into a liquid electrolyte.[24] Moreover, most of the polyanion hosts have used only the Mn^{3+}/Mn^{2+} couples; the limited number operating on the Mn^{4+}/Mn^{3+} couple have provided little interest. The Mn^{4+}/Mn^{3+} couple in Li₂MnP₂O₇ is located at a voltage that oxidizes conventional organic-liquid electrolytes.[25] The Mn^{4+}/Mn^{3+} couple is only partially (30%) active in Na₃MnPO₄CO₃ and cannot be accessed in Na₄MnV(PO₄)₃ from which the extraction of Na⁺ ions proceeds in the sequences of the V^{4+}/V^{3+}, Mn^{3+}/Mn^{2+}, and V^{5+}/V^{4+} redox couples from the low to the high voltage.[26,27] Very little cycle stability was obtained in Na₃MnTi(PO₄)₃ and Na₃Co₀.₅Mn₀.₅Ti(PO₄)₃.[28,29]

In order to reduce the concentration of Mn in a polyanion framework structure to where the cooperative Jahn−Teller distortion does not occur with all Mn^{3+} and the surface disproportionation of the Mn^{3+} to Mn^{2+} and Mn^{4+} might be

suppressed, we have investigated as a sodium cathode $Na_3MnZr(PO_4)_3$ having the rhombohedral NASICON structure. In an early report, the measurement of ionic conductivity of $Na_3MnZr(PO_4)_3$ revealed that the rhombohedral phase of $Na_3MnZr(PO_4)_3$ has an activation energy of 0.38 eV, which is similar to the activation energies of rhombohedral phases of $Na_3V_2(PO_4)_3$ (0.34 eV) and $Na_3Cr_2(PO_4)_3$ (0.39 eV) and considerably smaller than the activation energies of the monoclinic phases of $Na_3V_2(PO_4)_3$ (0.87 eV) and $Na_3Cr_2(PO_4)_3$ (0.62 eV), suggesting its potential suitability as a cathode for sodium batteries.[30−33] However, in this early study, $Na_3MnZr(PO_4)_3$ was not investigated electrochemically as a cathode material of a sodium battery.[30] A subsequent study failed to obtain a reversible extraction of Na^+ from $Na_3MnZr(PO_4)_3$ synthesized by solid-state reaction and uncoated by carbon or any other electronic conductor, which has led to the suggestion that the problem is an instability of the octahedral-site Mn^{3+} ion.[33] Such an instability could be due to a cooperative Jahn−Teller distortion or to a surface disproportionation $2Mn^{3+} = Mn^{2+} + Mn^{4+}$ with Mn^{2+} dissolution in the liquid electrolytes. The failure to extract Na^+ reversibly was the result of a solid-state synthesis that gives micron-sized crystallites and a failure to coat the active electrode material that is an electronic insulator with a carbon coat, or a coat of another electronic conductor that also allows Na^+ cross over.[34−36] In this paper, we have used a sol−gel synthesis to obtain 200 nm particles of $Na_3MnZr(PO_4)_3$ that were coated *in situ* with a thin carbon layer. With these particles, we were able to extract/insert Na^+ ions reversibly over a large solid-solution range, accessing not only the Mn^{3+}/Mn^{2+} redox couple but also the Mn^{4+}/Mn^{3+} redox couple at, respectively, 3.5 and 4.0 V versus Na^+/Na. Moreover, the cathode showed no cooperative Jahn−Teller distortion down to lowest temperatures and it can be cycled stably over many cycles indicating no evidence of surface disproportionation and Mn^{2+} dissolution. Moreover, we report a theoretical analysis of the Na^+-ion extraction sites in the rhombohedral NASICON-structured cathode $Na_3MnZr(PO_4)_3$ containing two quite different octahedral-site transition-metal cations whereas earlier theoretical studies have been confined to NASICON structures with only one octahedral-site transition-metal cation. The first-principles calculations also demonstrate the intrinsic stability of the $Na_3MnZr(PO_4)_3$ structure during desodiation in addition to the changes in the local Mn environment.

■ RESULTS AND DISCUSSION

Synthesis and Crystal Structure of $Na_3MnZr(PO_4)_3$. A sol−gel method was used to prepare the cathode material $Na_3MnZr(PO_4)_3$; the resulting material had a particle size of about 200 nm (Figure 1a). A thin layer of carbon was coated on the surface of $Na_3MnZr(PO_4)_3$ particles during the synthesis procedure to provide electron tunneling to the surface Na^+ ions with subsequent oxidation of the Mn^{2+} to Mn^{3+} and, eventually, to Mn^{4+} (Figure 1b); the amount of coated carbon was about 7.1% according to thermogravimetric analysis (Figure S1). The crystalline region of the cathode material exhibited lattice fringes with an interplanar spacing of about 0.64 nm, consistent with the (012) atomic planes of $Na_3MnZr(PO_4)_3$ with the rhombohedral structure (Figure 1c).

A Rietveld refinement of the X-ray diffraction (XRD) pattern further confirmed the formation of $Na_3MnZr(PO_4)_3$ with the rhombohedral NASICON structure in the space group $R\bar{3}c$ (Figure 1d).[30,37] The absence of additional peaks
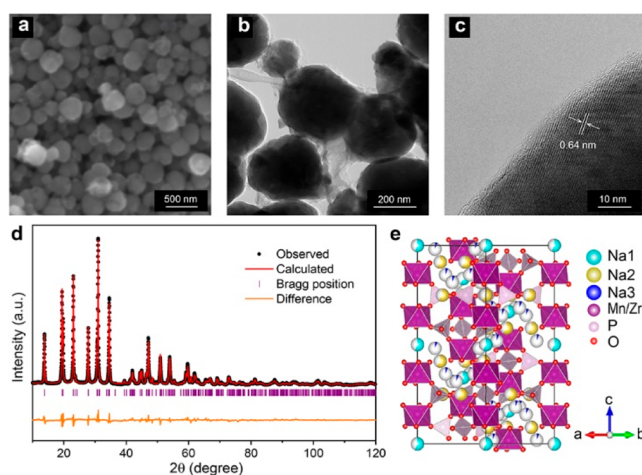

Figure 1. (a) SEM image, (b) TEM image, (c) high-resolution TEM image, (d) XRD pattern and Rietveld refinement, and (e) crystal structure of the cathode material $Na_3MnZr(PO_4)_3$.

corresponding to long-range ordering between Mn and Zr in the XRD pattern indicates the octahedral sites were randomly occupied by the two kinds of transition metals in the NASICON framework.[38,39] The lattice parameters of $Na_3MnZr(PO_4)_3$ (a = 8.988 Å, and c = 22.594 Å) are larger than those of the well-documented $Na_3V_2(PO_4)_3$ cathode for sodium batteries (a = 8.738 Å, and c = 21.815 Å),[40] which provides sufficient interstitial volume for extraction/insertion of Na^+ ions. The Rietveld refinement revealed the occupancy factors of 0.558, 0.596, and 0.066 for Na(1), Na(2), and Na(3) sites, respectively, corresponding to 16.45 (6 × 0.558 + 18 × 0.596 + 36 × 0.066) Na^+ ions per unit-cell (Z = 6), consistent with the expected chemical formula $Na_3MnZr(PO_4)_3$ (Table S1).

The crystal structure of $Na_3MnZr(PO_4)_3$ is composed of MnO_6 and ZrO_6 octahedral units bridged by corner-sharing PO_4 tetrahedral units to establish a framework structure with interstitial sites accommodating three different types of Na^+ ions: (i) the Na(1) sites with 6-fold coordination, (ii) the Na(2) sites with 8-fold coordination, and (iii) the Na(3) sites which are four-coordinate (NaO_4) sites situated in-between the Na(1) and Na(2) sites (Figure 1e). An occupancy of Na(1) sites less than unity in the Rietveld refinement suggested that a portion of Na^+ ions at Na(1) sites are displaced to the Na(3) sites, which has been observed in similar NASICON structures and suggests that simultaneous occupation of neighboring Na(1) and Na(2) sites by Na^+ ions results in a Coulombic repulsion that displaces a Na^+ ion from the Na(1) site to a Na(3) site.[41] The electrochemical activities of NASICON-structured materials are typically from extraction/insertion of Na^+ ions located at Na(2) sites.[42,43] As is detailed in the following sections, the energies of the Na(1) and Na(2) sites are affected by the local Mn and Zr ordering. A theoretical capacity of 107 mAh g^{-1} could be obtained for $Na_3MnZr(PO_4)_3$ through utilization of both the Mn^{3+}/Mn^{2+} and Mn^{4+}/Mn^{3+} redox couples with extraction/insertion of two Na^+ ions at Na(2) sites per formula unit.

Electrochemical Performance of $Na_3MnZr(PO_4)_3$. Two oxidation peaks at 3.6 and 4.1 V are revealed in the cyclic voltammetry profiles of the $Na_3MnZr(PO_4)_3$ cathode, corresponding to the reversible extraction of two Na^+ ions accompanied by the successive two-phase transformations

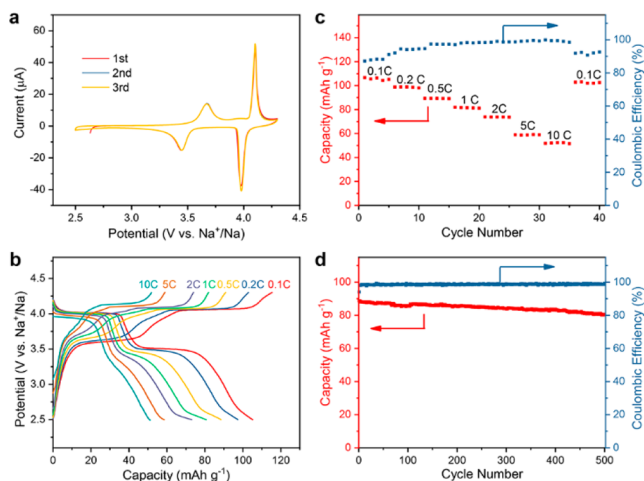from $Na_3MnZr(PO_4)_3$ to $Na_2MnZr(PO_4)_3$ and then to $NaMnZr(PO_4)_3$ (Figure 2a). The two reduction peaks located

Figure 2. Electrochemical performance of the $Na_3MnZr(PO_4)_3$ cathode. (a) Cyclic voltammetry profiles at a scan rate of 1 mV s^{-1}. (b) Charge/discharge profiles at rates from 0.1 to 10 C. (c) Discharge capacities and Coulombic efficiencies at rates from 0.1 to 10 C. (d) Charge/discharge cycling performance at 0.5 C rate.

at 4.0 and 3.5 V can be attributed to the successive Mn^{4+}/Mn^{3+} and Mn^{3+}/Mn^{2+} redox couples, accompanied by the transformations from $NaMnZr(PO_4)_3$ to $Na_2MnZr(PO_4)_3$ and then back to $Na_3MnZr(PO_4)_3$. The charge profile of the cathode exhibits a voltage plateau at 3.6 V corresponding to the extraction of the first Na$^+$ ion through the Mn^{3+}/Mn^{2+} redox couple followed by another voltage plateau at 4.1 V corresponding to the extraction of the second Na$^+$ ion through the Mn^{4+}/Mn^{3+} redox couple (Figure 2b). Upon discharge, the two plateaus located at 4.0 and 3.5 V represent the insertion of two Na$^+$ ions through the Mn^{4+}/Mn^{3+} and Mn^{3+}/Mn^{2+} redox couples, respectively. As a cathode material for sodium batteries, $Na_3MnZr(PO_4)_3$ delivers discharge voltage plateaus higher than the well-documented NASICON compounds $Na_3V_2(PO_4)_3$ (3.4 V) and $NaTi_2(PO_4)_3$ (2.1 V).[44,45] Moreover, the Mn^{4+}/Mn^{3+} redox couple in $Na_3MnZr(PO_4)_3$ provides a discharge voltage (4.0 V) higher than the well-documented Mn^{3+}/Mn^{2+} redox couple in other manganese phosphate cathodes, such as $Na_2MnP_2O_7$ (3.6 V) and $Na_4Mn_3(PO_4)_2P_2O_7$ (3.8 V) for sodium batteries.[46−48]

The discharge capacity of $Na_3MnZr(PO_4)_3$ was 105 mAh g^{-1} at 0.1 C rate, which is close to the theoretical capacity (107 mAh g^{-1}) corresponding to extraction/insertion of two Na$^+$ ions per formula unit (Figure 2c). When the rate increased to 1 and 10 C, the discharge capacity of the cathode was 82 and 52 mAh g^{-1}, respectively. The low Coulombic efficiency at the low rate (∼90% at 0.1 C) is most probably from the oxidation of the liquid electrolyte at the high charging voltage (4.3 V);[49−51] however, $Na_3MnZr(PO_4)_3$ still exhibits an initial Coulombic efficiency (87%), higher than that of other manganese phosphate cathodes for sodium batteries, such as $Na_2MnP_2O_7$ (69%), $Na_4Mn_3(PO_4)_2P_2O_7$ (60%), and Na_2MnPO_4F (80%).[48,52,53] When the current density went back to the initial 0.1 C rate, the discharge capacity of the cathode returned to the value of 104 mAh g^{-1}, demonstrating a useful rate capability of the cathode. In addition, an excellent cycling stability was obtained for $Na_3MnZr(PO_4)_3$; 91% of the

initial capacity could be retained after 500 cycles at 0.5 C rate with an average Coulombic efficiency of 98.7% (Figure 2d). In terms of discharge voltage, reversible capacity, and cycling stability, $Na_3MnZr(PO_4)_3$ gives a performance superior to that of other manganese phosphate cathodes for sodium batteries reported in the literature (Table S2). The XRD pattern and TEM image of the cathode after the charge/discharge cycling tests were almost identical to those of the pristine one (Figure S2), which implies that the crystal structure of $Na_3MnZr(PO_4)_3$ was well-maintained after repeated extraction/insertion of Na$^+$ ions.

Desodiation Mechanism of $Na_3MnZr(PO_4)_3$. In order to understand further changes in the structure during desodiation, the energies of $Na_xMnZr(PO_4)_3$ structures from x = 1−3 were computed with DFT. The convex hull shows the formation energy per formula unit (E_{form}) of $Na_xMnZr(PO_4)_3$ phases relative to the end member compositions of $Na_3MnZr(PO_4)_3$ (E_{Na3}) and $NaMnZr(PO_4)_3$ (E_{Na1}) according to the formula $E_{form} = E_{Nax} - 1/2(x-1) E_{Na3} - 1/2(3-x) E_{Na1}$ (Figure 3a).

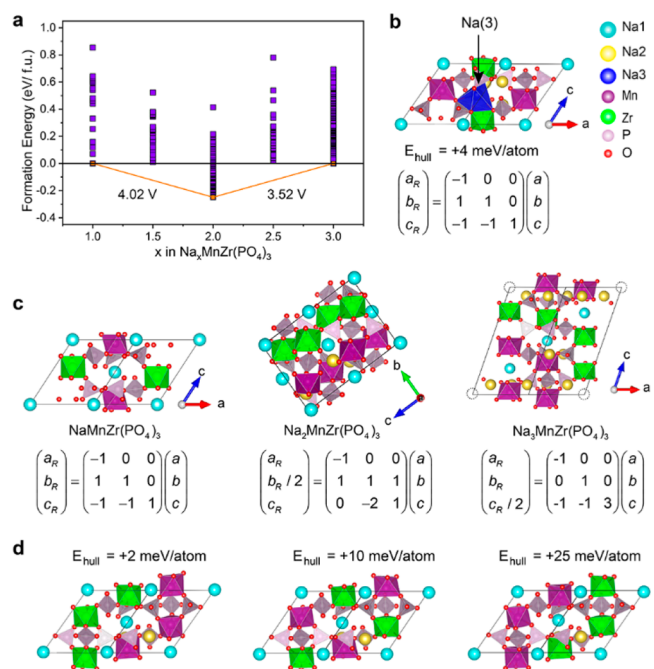**Figure 3.** (a) Convex hull of $Na_xMnZr(PO_4)_3$ from DFT calculations. (b) Near hull DFT relaxed structure of $Na_3MnZr(PO_4)_3$ containing a Na$^+$ ion in a Na(3) site. (c) Structures of the lowest energy phase of $Na_xMnZr(PO_4)_3$ and the relationship between the unit cell parameters (a, b, c) of the DFT cells and the corresponding unit cell parameters of the $R\bar{3}c$ structure (a_R, b_R, c_R). Na(1) vacancies are shown as dashed circles. (d) DFT optimized structures of $Na_2MnZr(PO_4)_3$ with different Mn/Zr orderings.

$Na_2MnZr(PO_4)_3$ is a stable phase on the hull between the end member configurations, and the intermediate configurations at $Na_{1.5}MnZr(PO_4)_3$ and $Na_{2.5}MnZr(PO_4)_3$ are metastable/unstable. Two-phase reactions between $Na_3MnZr(PO_4)_3$ and $Na_2MnZr(PO_4)_3$ and between $Na_2MnZr(PO_4)_3$ and $NaMnZr(PO_4)_3$ are therefore preferred, in accordance with XRD analysis in the following section. From the lowest energy structures, sequential reactions from $Na_3MnZr(PO_4)_3 \rightarrow Na_2MnZr(PO_4)_3$ and $Na_2MnZr(PO_4)_3 \rightarrow NaMnZr(PO_4)_3$ were predicted to occur at 3.52 and 4.02 V based on the approach of Aydinol et al.,[54] in good agreement with the

experimentally observed charge plateaus at 3.6 and 4.1 V. The energy of the $Na_xMnZr(PO_4)_3$ structures on the hull (x = 1, 2, and 3) were compared to all phases in the Na−Mn−Zr−P−O phase diagram in the Materials Project,[55] and all of the structures were found to be stable with respect to decomposition to neighboring phases of $NaMnPO_4$, $NaZr_2(PO_4)_3$, $Na_4P_2O_7$, $NaPO_3$, $MnPO_4$, and ZrO_2, highlighting the stability of the desodiated $Na_xMnZr(PO_4)_3$ structure.

For the end member composition of $Na_3MnZr(PO_4)_3$, the small energy difference between the structures above the hull predicated with DFT calculations (E_{hull} = 1−35 meV/atom) suggests that there is significant disorder between the Mn and Zr sites within the structure. At the local scale, the distribution of Mn and Zr sites in $Na_3MnZr(PO_4)_3$ leads to three possible types of Na(1) site that share faces with either two MnO_6, two ZrO_6 or one MnO_6 and one ZrO_6 octahedron along the c-axis. In the lowest energy structure of $Na_3MnZr(PO_4)_3$, the MnO_6−Na(1)−MnO_6 and MnO_6−Na(1)−ZrO_6 sites are occupied, whereas the ZrO_6−Na(1)−ZrO_6 sites are vacant (Figure 3c). This result suggests that the unfavorable electrostatic interaction between Zr^{4+} and Na^+ may locally destabilize ZrO_6−Na(1)−ZrO_6 configurations in $Na_3MnZr(PO_4)_3$. This finding is consistent with the structural refinement in which the occupancy of the Na(1) sites was less than unity. During structural optimization of several low energy structures, Na^+ ions initially located in a ZrO_6−Na(1)−ZrO_6 configurations relaxed to the intermediate four coordinated (NaO_4) sites situated between the Na(1) and Na(2) sites (Figure 3b), in accordance with the Rietveld refinement. The formation energy of the structure was only 4 meV/atom above the lowest energy structure, which suggests that these Na(3) sites may act as additional low-energy positions to accommodate Na^+ ions in the $Na_3MnZr(PO_4)_3$ structure.

In the $Na_3MnZr(PO_4)_3$ structures, the Na^+ ions occupy the Na(2) sites that are face sharing with either two Mn^{2+} or one Mn^{2+} and one Zr^{4+} octahedron, as a result of the smaller electrostatic repulsion of Mn^{2+}−Na^+ interactions compared with Zr^{4+}−Na^+ interactions. The high energy, ZrO_6−Na(2)−ZrO_6 local configurations are therefore preferential sites for Na(2) vacancies. For a random distribution of Mn/Zr ions, the ZrO_6−Na(2)−ZrO_6 configurations account for 1/4 of the total Na(2) vacant sites. As approximately 1/3 of the total Na(2) sites are vacant in $Na_3MnZr(PO_4)_3$, the remaining 1/12 of Na(2) vacancies will preferentially occur in MnO_6−Na(2)−ZrO_6 configurations rather than in MnO_6−Na(2)−MnO_6 configurations, based on the previous electrostatic arguments and analysis of the low energy structures. The energies of the structures are also sensitive to the local Na ordering due to Na^+−Na^+ interactions. However, the random distribution of Mn/Zr ions and high energy of the ZrO_6−Na(2)−ZrO_6 sites precludes the formation of long-range Na orderings, such as that observed in the rhombohedral structure of $Na_3V_2(PO_4)_3$.[56]

Analogous to $Na_3MnZr(PO_4)_3$, there is a weak preference for Mn^{3+}/Zr^{4+} ordering in $Na_2MnZr(PO_4)_3$ (Figure 3d). While the lowest energy structure of $Na_2MnZr(PO_4)_3$ had fully occupied Na(1) sites, the Na(1) sites along ZrO_6−Na(1)−ZrO_6 or ZrO_6−Na(1)−MnO_6 configurations are also less stable than MnO_6−Na(1)−MnO_6 configurations, and Na^+ ions in ZrO_6−Na(1)−ZrO_6 or ZrO_6−Na(1)−MnO_6 configurations in several structures relaxed to Na(3) sites during the structural optimization, leading to vacant Na(1) sites along

either ZrO_6−Na(1)−ZrO_6 or ZrO_6−Na(1)−MnO_6 configurations. Na^+ ions occupy 1/3 of the Na(2) sites in $Na_2MnZr(PO_4)_3$, and the site containing a MnO_6−Na(2)−MnO_6 configuration will be preferentially occupied because of the lower energy than the site containing a Na(2) ion in a MnO_6−Na(2)−ZrO_6 or ZrO_6−Na(2)−ZrO_6 configuration.

For the $NaMnZr(PO_4)_3$ end member, all of the Mn sites are oxidized to Mn^{4+}. In the lowest energy structure, the Na(1) sites are fully occupied whereas the Na(2) sites are unoccupied. In the small unit cell structures that initially contained vacancies in MnO_6−Na(1)−MnO_6 or ZrO_6−Na(1)−ZrO_6 configurations, adjacent Na^+ ions in Na(2) sites relaxed to occupy the Na(1) sites. The lowest energy structure containing a ZrO_6−Na(1)−MnO_6 vacancy was 18 meV/atom above the hull, suggesting that there is a strong preference for full occupancy of the Na(1) sites in $NaMnZr(PO_4)_3$.

From these results, a tentative mechanism for the desodiation of $Na_3MnZr(PO_4)_3$ can be proposed. On initial desodiation from $Na_3MnZr(PO_4)_3$ to $Na_2MnZr(PO_4)_3$ at 3.6 V, Na^+ ions are preferentially extracted from the partially occupied MnO_6−Na(2)−ZrO_6 sites while MnO_6−Na(2)−MnO_6 sites remain fully occupied. The Na^+ ions in local MnO_6−Na(1)−MnO_6 environments remain fully occupied in both $Na_3MnZr(PO_4)_3$ and $Na_2MnZr(PO_4)_3$. The occupation of ZrO_6−Na(1)−ZrO_6 sites increases on desodiation to $Na_2MnZr(PO_4)_3$, although displacement of Na(1) ions to Na(3) sites may also take place more easily due to the increase in the number of Na(2) vacancies. On further desodiation to $NaMnZr(PO_4)_3$ at 4.1 V, the Na(1) sites become fully occupied, while the Na(2) sites are fully unoccupied.

Structural Evolution of $Na_3MnZr(PO_4)_3$. The phase transition of $Na_3MnZr(PO_4)_3$ during extraction/insertion of Na^+ ions was investigated by *ex situ* XRD analysis (Figure 4a).

Figure 4. (a) XRD patterns of the $Na_3MnZr(PO_4)_3$ cathode at different states of charge and discharge. (b) Variation of lattice parameters of $Na_xMnZr(PO_4)_3$ structures. (c) Variation of volume of $Na_xMnZr(PO_4)_3$ structures.

A two-phase transformation from $Na_3MnZr(PO_4)_3$ to $Na_2MnZr(PO_4)_3$ was observed on extraction of the first Na^+ ion, followed by another two-phase transformation process from $Na_2MnZr(PO_4)_3$ to $NaMnZr(PO_4)_3$ on extraction of the second Na^+ ion. The phase transition of $Na_3MnZr(PO_4)_3$ is accompanied by the changes in the unit cell parameters

(Figure 4b), which are closely linked to the occupation of the Na(1) and Na(2) sites.[57,58]

There is a small overall increase in the *c*-lattice parameter during desodiation (0.1%), in agreement with the DFT calculation (0.4%) from the supercell containing 8 formula units of $Na_xMnZr(PO_4)_3$ with disordered Mn and Zr sites (Figure S3). It is known from previous studies that the presence of Na(1) vacancies leads to an expansion of the *c*-axis.[59] $Na_3MnZr(PO_4)_3$ contains Na(1) vacancies at the ZrO_6–Na(1)–ZrO_6 sites. On desodiation to $Na_2MnZr(PO_4)_3$, one of the Na^+ ions remained in a ZrO_6–Na(1)–ZrO_6 site, while the other Na(1) site was empty as the Na^+ ion occupied an adjacent Na(3) site. On desodiation to $NaMnZr(PO_4)_3$, the Na(1) sites are filled and there is a small increase in the *c*-lattice parameter, which has previously been ascribed to an increased repulsion of the transition metals (i.e., Mn^{4+}–Mn^{4+} vs Mn^{2+}–Mn^{2+}) along the *c*-axis at higher states of charge. The small overall change in the *c*-lattice parameter observed experimentally during desodiation is related to the competing effects of transition metal repulsion causing expansion and increasing Na(1) site occupation causing contraction.

The small increase in the *c*-lattice parameter during desodiation is accompanied by a decrease in the *a*-lattice parameters and therefore an increase of *c/a* ratio. The decrease in the *a*-lattice parameter is commonly ascribed to a decrease in the Na(2) site occupation and a decrease in the effective ionic radius of the transition metal during oxidation, which for the current system are 0.83, 0.645, 0.53 Å for Mn^{2+}, Mn^{3+}, and Mn^{4+}, respectively.[60] The overall decrease in the *a*-lattice parameter observed experimentally (2.8%) is smaller than predicted from the supercell (5.1%) and the lowest energy structures in the convex hull (5.9%), which may be due to the residual transition-metal ordering in the calculated structures in addition to the lack of temperature effects in the nominally 0 K DFT calculations. Moreover, $Na_3MnZr(PO_4)_3$ has a smaller volume change (5.5%) on desodiation to $NaMnZr(PO_4)_3$ than other cathode materials, such as $Na_4Mn_3(PO_4)_2P_2O_7$ (~7%) and $Na_3V_2(PO_4)_3$ (~8.3%) for sodium batteries, and $LiFePO_4$ (~6.8%) for lithium batteries (Figure 4c).[52,61,62] In general, the small variation in the *a* and *c* lattice parameters and the small volume change of $Na_3MnZr(PO_4)_3$ is key to the long-term cycling stability.

The oxidation states of Mn and Zr in the $Na_3MnZr(PO_4)_3$ electrode was probed by X-ray photoelectron spectroscopy (XPS) at different states of charge (Figure S4). The binding energy of Mn 3p located at 48.8 eV before charging is in agreement with the presence of Mn^{2+} in the pristine $Na_3MnZr(PO_4)_3$ electrode. The binding energy of Mn 3p increased to 49.5 eV after charging the electrode to 3.9 V, indicating the oxidation of Mn^{2+} to Mn^{3+}. At the end of charging the electrode to 4.3 V, the binding energy of Mn 3p further increased to 50.2 eV, implying the oxidation of Mn^{3+} to Mn^{4+}.[63] The binding energies of Zr 3d remained unchanged in the charging process, which suggests that the extraction/insertion of Na^+ ions proceeds through utilization of the Mn^{3+}/Mn^{2+} and Mn^{4+}/Mn^{3+} redox couples, keeping the valence state of Zr^{4+} unchanged. The change in the oxidation state is further supported by calculation of the magnetic moment on the Mn and Zr sites of the lowest energy structures in the convex hull through a Bader analysis (Table S3).[64] The magnetic moment on Zr remains zero through-out the desodiation process and the charge remains approximately constant at +2.70 e, consistent with a fixed Zr^{4+} oxidation state with a *d*-electron

configuration of d^0. The change in the magnetic moment on Mn is consistent with the oxidation of high-spin Mn^{2+} (d^5) to Mn^{3+} (d^4) from $Na_3MnZr(PO_4)_3$ → $Na_2MnZr(PO_4)_3$, followed by the oxidation of Mn^{3+} to Mn^{4+} (d^3) from $Na_2MnZr(PO_4)_3$ → $NaMnZr(PO_4)_3$.

Inhibited Cooperative Jahn–Teller Distortion of Manganese. As all of the manganese ions in the $Na_2MnZr(PO_4)_3$ structure are in the Mn^{3+} oxidation state, it may be expected that the octahedral MnO_6 centers would undergo a positive (negative) Jahn–Teller distortion in which two (four) of the Mn–O bond are lengthened and four (two) of the Mn–O bonds are shortened, as is observed in other Mn^{3+} systems.[65−67] There are two distinct O sites in the rhombohedral NASICON structure: O1 and O2 (Figure 5a).
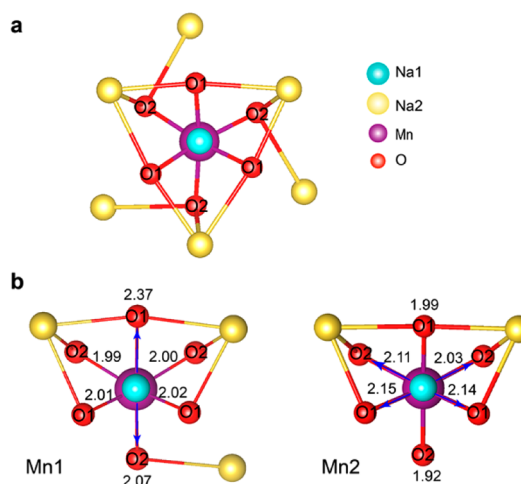

Figure 5. (a) Local bonding environment around MnO_6 site. (b) Coordination of two Mn sites, Mn1 and Mn2, in the lowest energy structure of $Na_2MnZr(PO_4)_3$. Mn–O bond lengths are shown in Å between the Mn sites and the two distinct O sites in the structure, O1 and O2. Jahn–Teller lengthened bonds are highlighted with blue arrows.

The O1 ions are located in between the Mn (or Zr) and Na(1) sites, forming the common faces between the MnO_6 and NaO_6 octahedra. The O2 sites are on the opposite side of the MnO_6 (or ZrO_6) octahedra along the *c*-direction of the rhombohedral cell.

In the lowest energy $Na_2MnZr(PO_4)_3$ structure, MnO_6 centers have two different local environments (Mn1 and Mn2). For the Mn1 configuration, four of the Mn1−O bonds are shortened (S) from the average bond length of 2.08 Å and two Mn1−O bonds are lengthened (L), which is consistent with a positive Jahn−Teller distortion, however, there is significant deviation between the Mn1−O1 and Mn1−O2 bond lengths (Figure 5b). The Mn1−O1(L) bond, which shares a common O1 with two Na(2) sites, is considerably longer (2.37 Å) than the Mn1−O2(L) bond (2.07 Å) on the opposite site of the MnO_6 octahedron that shares a common O1 with one Na(2). The Mn1−O1(S) bonds in the plane perpendicular to the Mn1−O(L) bond are also slightly shorter than the Mn1−O2(S) bonds. The distribution of bond lengths is different for the Mn2 site; there are two Mn2−O(S) bonds and four Mn2−O(L) bonds, consistent with a negative Jahn−Teller distortion. As was the case for the Mn1 configuration, the Mn2−O1 bonds are longer than the Mn2−O2 bonds. Comparing the bond distributions of the two Mn sites, it

appears that the orientation of the local Jahn—Teller distortion is subtly related to the local Na ordering, in which there is a preference to maximize the number of Jahn—Teller lengthened bonds that share common oxygens with Na(2) sites. Although the MnO_6 sites are distorted on the local scale, the lack of long-range ordering of the Na(2) sites suggests that a cooperative Jahn—Teller distortion of the Mn^{3+} centers as observed in other materials will be inhibited, which is beneficial for the long-term cycling stability.

CONCLUSIONS

In conclusion, the NASICON-structured $Na_3MnZr(PO_4)_3$ with three-dimensional channels for reversible extraction/insertion of Na^+ ions is able to be cycled through a stable Mn^{3+} composition $Na_2MnZr(PO_4)_3$ to give access to both the Mn^{4+}/Mn^{3+} and Mn^{3+}/Mn^{2+} mixed-valent two-phase states. The octahedral sites at the Mn^{3+} are distorted by different local environments, not by a cooperative Jahn—Teller distortion that removes an orbital degeneracy. Moreover, a cooperative surface disproportionation reaction of Mn^{3+} is also suppressed, as there is no evidence of a Mn^{2+} dissolution into an organic liquid-carbonate electrolyte. On reversible extraction/insertion of two Na^+ ions per formula unit, the voltage profile shows two plateaus, one for a two-phase Mn^{4+}/Mn^{3+} couple at 4.0 V and the other for a two-phase Mn^{3+}/Mn^{2+} couple at 3.5 V versus Na^+/Na with a step change at the Mn^{3+} composition $Na_2MnZr(PO_4)_3$. This high-voltage cathode for a sodium battery is superior to other manganese-phosphate cathodes reported in the literature, including an earlier study that failed to extract Na^+ ions reversibly from $Na_3MnZr(PO_4)_3$. The stability of the Mn^{3+} phase $Na_2MnZr(PO_4)_3$ and the local occupation of Na^+ sites which was similar to that in NASICON structures with a single octahedral-site cation have been reproduced by DFT calculations. Nevertheless, still to be explored is the role of electron tunneling from/to a surface coat to/from surface Na^+ ions in both the Na^+ extraction/insertion reactions and the penetration of electrons between Mn ions separated by $(PO_4)^{3-}$ anions.

ASSOCIATED CONTENT

ⓢ Supporting Information

The Supporting Information is available free of charge on the ACS Publications website at DOI: 10.1021/jacs.8b11388.

> Experimental details; computational methodology; TGA of the cathode material; XRD pattern and TEM image of the cycled cathode; structure of supercells for DFT calculations; XPS spectra of the cathode at different charging state; crystallographic data of the cathode material; comparison with other cathode materials; magnetic moment and Bader charge calculations (PDF)

AUTHOR INFORMATION

Corresponding Author

*jgoodenough@mail.utexas.edu

ORCID ⓘ

Hongcai Gao: 0000-0002-3671-8765
Sen Xin: 0000-0002-0546-0626
Leigang Xue: 0000-0002-7359-7915
Graeme Henkelman: 0000-0002-0336-7153
John B. Goodenough: 0000-0001-9350-3034

Author Contributions

#H. Gao and I. D. Seymour contributed equally to this work.

Notes

The authors declare no competing financial interest.

REFERENCES

(1) Goodenough, J. B. Evolution of strategies for modern rechargeable batteries. *Acc. Chem. Res.* **2013**, *46*, 1053−1061.
(2) Larcher, D.; Tarascon, J. M. Towards greener and more sustainable batteries for electrical energy storage. *Nat. Chem.* **2015**, *7*, 19−29.
(3) Yabuuchi, N.; Kubota, K.; Dahbi, M.; Komaba, S. Research development on sodium-ion batteries. *Chem. Rev.* **2014**, *114*, 11636−11682.
(4) Palomares, V.; Serras, P.; Villaluenga, I.; Hueso, K. B.; Carretero-Gonzalez, J.; Rojo, T. Na-ion batteries, recent advances and present challenges to become low cost energy storage systems. *Energy Environ. Sci.* **2012**, *5*, 5884−5901.
(5) Kundu, D.; Talaie, E.; Duffort, V.; Nazar, L. F. The emerging chemistry of sodium ion batteries for electrochemical energy storage. *Angew. Chem., Int. Ed.* **2015**, *54*, 3431−3448.
(6) Goodenough, J. B. Energy storage materials: A perspective. *Energy Storage Mater.* **2015**, *1*, 158−161.
(7) Han, M. H.; Gonzalo, E.; Singh, G.; Rojo, T. A comprehensive review of sodium layered oxides: powerful cathodes for Na-ion batteries. *Energy Environ. Sci.* **2015**, *8*, 81−102.
(8) Fang, C.; Huang, Y. H.; Zhang, W. X.; Han, J. T.; Deng, Z.; Cao, Y. L.; Yang, H. X. Routes to high energy cathodes of sodium-ion batteries. *Adv. Energy Mater.* **2016**, *6*, 1501727.
(9) Wang, P. F.; You, Y.; Yin, Y. X.; Guo, Y. G. Layered oxide cathodes for sodium-ion batteries: Phase transition, air stability, and performance. *Adv. Energy Mater.* **2018**, *8*, 1701912.
(10) Wang, L.; Lu, Y. H.; Liu, J.; Xu, M. W.; Cheng, J. G.; Zhang, D. W.; Goodenough, J. B. A superior low-cost cathode for a Na-ion battery. *Angew. Chem., Int. Ed.* **2013**, *52*, 1964−1967.
(11) Lee, H. W.; Wang, R. Y.; Pasta, M.; Lee, S. W.; Liu, N.; Cui, Y. Manganese hexacyanomanganate open framework as a high-capacity positive electrode material for sodium-ion batteries. *Nat. Commun.* **2014**, *5*, 5280.
(12) You, Y.; Wu, X. L.; Yin, Y. X.; Guo, Y. G. High-quality Prussian blue crystals as superior cathode materials for room-temperature sodium-ion batteries. *Energy Environ. Sci.* **2014**, *7*, 1643−1647.
(13) Song, J.; Wang, L.; Lu, Y. H.; Liu, J.; Guo, B. K.; Xiao, P. H.; Lee, J. J.; Yang, X. Q.; Henkelman, G.; Goodenough, J. B. Removal of interstitial H2O in hexacyanometallates for a superior cathode of a sodium-ion battery. *J. Am. Chem. Soc.* **2015**, *137*, 2658−2664.
(14) Liu, Y.; Qiao, Y.; Zhang, W. X.; Li, Z.; Ji, X.; Miao, L.; Yuan, L. X.; Hu, X. L.; Huang, Y. H. Sodium storage in Na-rich NaxFeFe-(CN)6 nanocubes. *Nano Energy* **2015**, *12*, 386−393.
(15) Singh, P.; Shiva, K.; Celio, H.; Goodenough, J. B. Eldfellite, NaFe(SO4)2: An intercalation cathode host for low-cost Na-ion batteries. *Energy Environ. Sci.* **2015**, *8*, 3000−3005.
(16) Kim, H.; Park, I.; Seo, D. H.; Lee, S.; Kim, S. W.; Kwon, W. J.; Park, Y. U.; Kim, C. S.; Jeon, S.; Kang, K. New iron-based mixed-polyanion cathodes for lithium and sodium rechargeable batteries: Combined first principles calculations and experimental study. *J. Am. Chem. Soc.* **2012**, *134*, 10369−10372.

(17) Lim, S. Y.; Kim, H.; Chung, J.; Lee, J. H.; Kim, B. G.; Choi, J. J.; Chung, K. Y.; Cho, W.; Kim, S. J.; Goddard, W. A.; Jung, Y.; Choi, J. W. Role of intermediate phase for stable cycling of Na7V4(P2O7)-4PO4 in sodium ion battery. *Proc. Natl. Acad. Sci. U. S. A.* **2014**, *111*, 599−604.

(18) Qi, Y. R.; Mu, L. Q.; Zhao, J. M.; Hu, Y. S.; Liu, H. Z.; Dai, S. Superior Na-storage performance of low-temperature-synthesized Na3(VO1-xPO4)2F1 + 2x (0 ≤ x ≤ 1) nanoparticles for Na-ion batteries. *Angew. Chem., Int. Ed.* **2015**, *54*, 9911−9916.

(19) Kawai, K.; Zhao, W. W.; Nishimura, S. I.; Yamada, A. High-voltage Cr4+/Cr3+ redox couple in polyanion compounds. *ACS Appl. Energy Mater.* **2018**, *1*, 928−931.

(20) Masquelier, C.; Croguennec, L. Polyanionic (phosphates, silicates, sulfates) frameworks as electrode materials for rechargeable Li (or Na) batteries. *Chem. Rev.* **2013**, *113*, 6552−6591.

(21) Barpanda, P.; Oyama, G.; Nishimura, S.; Chung, S. C.; Yamada, A. A 3.8-V earth-abundant sodium battery electrode. *Nat. Commun.* **2014**, *5*, 4358.

(22) Ong, S. P.; Chevrier, V. L.; Hautier, G.; Jain, A.; Moore, C.; Kim, S.; Ma, X. H.; Ceder, G. Voltage, stability and diffusion barrier differences between sodium-ion and lithium-ion intercalation materials. *Energy Environ. Sci.* **2011**, *4*, 3680−3688.

(23) Islam, M. S.; Fisher, C. A. J. Lithium and sodium battery cathode materials: computational insights into voltage, diffusion and nanostructural properties. *Chem. Soc. Rev.* **2014**, *43*, 185−204.

(24) Aravindan, V.; Gnanaraj, J.; Lee, Y. S.; Madhavi, S. LiMnPO4 - A next generation cathode material for lithium-ion batteries. *J. Mater. Chem. A* **2013**, *1*, 3518−3539.

(25) Zhou, H.; Upreti, S.; Chernova, N. A.; Hautier, G.; Ceder, G.; Whittingham, M. S. Iron and manganese pyrophosphates as cathodes for lithium-ion batteries. *Chem. Mater.* **2011**, *23*, 293−300.

(26) Chen, H. L.; Hao, Q.; Zivkovic, O.; Hautier, G.; Du, L. S.; Tang, Y. Z.; Hu, Y. Y.; Ma, X. H.; Grey, C. P.; Ceder, G. Sidorenkite (Na3MnPO4CO3): A New Intercalation Cathode Material for Na-Ion Batteries. *Chem. Mater.* **2013**, *25*, 2777−2786.

(27) Nisar, U.; Shakoor, R. A.; Essehli, R.; Amin, R.; Orayech, B.; Ahmad, Z.; Kumar, P. R.; Kahraman, R.; Al-Qaradawi, S.; Soliman, A. Sodium intercalation/de-intercalation mechanism in Na4MnV(PO4)-3 cathode materials. *Electrochim. Acta* **2018**, *292*, 98−106.

(28) Gao, H. C.; Li, Y. T.; Park, K.; Goodenough, J. B. Sodium extraction from NASICON-structured Na3MnTi(PO4)3 through Mn(III)/Mn(II) and Mn(IV)/Mn(III) redox couples. *Chem. Mater.* **2016**, *28*, 6553−6559.

(29) Wang, H. B.; Chen, C.; Qian, C.; Liang, C. D.; Lin, Z. Symmetric sodium-ion batteries based on the phosphate material of NASICON-structured Na3Co0.5Mn0.5Ti(PO4)3. *RSC Adv.* **2017**, *7*, 33273−33277.

(30) Feltz, A.; Barth, S. Preparation and conductivity behaviour of Na3MZr(PO4)3, (M: Mn, Mg, Zn). *Solid State Ionics* **1983**, *9−10*, 817−821.

(31) Novikova, S. A.; Larkovich, R. V.; Chekannikov, A. A.; Kulova, T. L.; Skundin, A. M.; Yaroslavtsev, A. B. Electrical conductivity and electrochemical characteristics of Na3V2(PO4)3-based NASICON-type materials. *Inorg. Mater.* **2018**, *54*, 794−804.

(32) Nogai, A. S.; Stefanovich, S. Y.; Bush, A. A.; Uskenbaev, D. E.; Nogai, A. A. Dipole ordering and ionic conductivity in nasicon-type Na3Cr2(PO4)3 structures. *Phys. Solid State* **2018**, *60*, 23−30.

(33) Pan, H. L.; Hu, Y. S.; Chen, L. Q. Room-temperature stationary sodium-ion batteries for large-scale electric energy storage. *Energy Environ. Sci.* **2013**, *6*, 2338−2360.

(34) Yuan, L. X.; Wang, Z. H.; Zhang, W. X.; Hu, X. L.; Chen, J. T.; Huang, Y. H.; Goodenough, J. B. Development and challenges of LiFePO4 cathode material for lithium-ion batteries. *Energy Environ. Sci.* **2011**, *4*, 269−284.

(35) Chen, S. Q.; Wu, C.; Shen, L. F.; Zhu, C. B.; Huang, Y. Y.; Xi, K.; Maier, J.; Yu, Y. Challenges and perspectives for NASICON-type electrode materials for advanced sodium-ion batteries. *Adv. Mater.* **2017**, *29*, 1700431.

(36) Wang, J. J.; Sun, X. L. Understanding and recent development of carbon coating on LiFePO4 cathode materials for lithium-ion batteries. *Energy Environ. Sci.* **2012**, *5*, 5163−5185.

(37) Cushing, B. L.; Goodenough, J. B. Li2NaV2(PO4)3: A 3.7 V lithium-insertion cathode with the rhombohedral NASICON structure. *J. Solid State Chem.* **2001**, *162*, 176−181.

(38) Rangan, K. K.; Gopalakrishnan, J. AM(V)M(III)(PO4)3: New mixed-metal phosphates having NASICON and related structures. *Inorg. Chem.* **1995**, *34*, 1969−1972.

(39) Patoux, S.; Rousse, G.; Leriche, J. B.; Masquelier, C. Structural and electrochemical studies of rhombohedral Na2TiM(PO4)3 and Li1.6Na0.4TiM(PO4)3 (M = Fe, Cr) phosphates. *Chem. Mater.* **2003**, *15*, 2084−2093.

(40) Jian, Z. L.; Zhao, L.; Pan, H. L.; Hu, Y. S.; Li, H.; Chen, W.; Chen, L. Q. Carbon coated Na3V2(PO4)3 as novel electrode material for sodium ion batteries. *Electrochem. Commun.* **2012**, *14*, 86−89.

(41) Boilot, J. P.; Collin, G.; Colomban, P. Crystal structure of the true NASICON: Na3Zr2Si2PO12. *Mater. Res. Bull.* **1987**, *22*, 669−676.

(42) Fang, Y. J.; Xiao, L. F.; Ai, X. P.; Cao, Y. L.; Yang, H. X. Hierarchical carbon framework wrapped Na3V2(PO4)3 as a superior high-rate and extended lifespan cathode for sodium-ion batteries. *Adv. Mater.* **2015**, *27*, 5895−5900.

(43) Song, W. X.; Cao, X. Y.; Wu, Z. P.; Chen, J.; Huangfu, K.; Wang, X. W.; Huang, Y. L.; Ji, X. B. A study into the extracted ion number for NASICON structured Na3V2(PO4)3 in sodium-ion batteries. *Phys. Chem. Chem. Phys.* **2014**, *16*, 17681−17687.

(44) Rui, X. H.; Sun, W. P.; Wu, C.; Yu, Y.; Yan, Q. Y. An advanced sodium-ion battery composed of carbon coated Na3V2(PO4)3 in a porous graphene network. *Adv. Mater.* **2015**, *27*, 6670−6676.

(45) Jiang, Y.; Shi, J. A.; Wang, M.; Zeng, L. C.; Gu, L.; Yu, Y. Highly reversible and ultrafast sodium storage in NaTi2(PO4)3 nanoparticles embedded in nanocarbon networks. *ACS Appl. Mater. Interfaces* **2016**, *8*, 689−695.

(46) Kim, H.; Yoon, G.; Park, I.; Hong, J.; Park, K. Y.; Kim, J.; Lee, K. S.; Sung, N. E.; Lee, S.; Kang, K. Highly stable iron- and manganese-based cathodes for long-lasting sodium rechargeable batteries. *Chem. Mater.* **2016**, *28*, 7241−7249.

(47) Barpanda, P.; Ye, T.; Avdeev, M.; Chung, S. C.; Yamada, A. A new polymorph of Na2MnP2O7 as a 3.6 V cathode material for sodium-ion batteries. *J. Mater. Chem. A* **2013**, *1*, 4194−4197.

(48) Park, C. S.; Kim, H.; Shakoor, R. A.; Yang, E.; Lim, S. Y.; Kahraman, R.; Jung, Y.; Choi, J. W. Anomalous manganese activation of a pyrophosphate cathode in sodium ion batteries: A combined experimental and theoretical study. *J. Am. Chem. Soc.* **2013**, *135*, 2787−2792.

(49) Gyenes, B.; Stevens, D. A.; Chevrier, V. L.; Dahn, J. R. Understanding anomalous behavior in coulombic efficiency measurements on Li-ion batteries. *J. Electrochem. Soc.* **2015**, *162*, A278−A283.

(50) Chen, L.; Dilena, E.; Paolella, A.; Bertoni, G.; Ansaldo, A.; Colombo, M.; Marras, S.; Scrosati, B.; Manna, L.; Monaco, S. Relevance of LiPF6 as etching agent of LiMnPO4 colloidal nanocrystals for high rate performing Li-ion battery cathodes. *ACS Appl. Mater. Interfaces* **2016**, *8*, 4069−4075.

(51) Choi, D. W.; Wang, D. H.; Bae, I. T.; Xiao, J.; Nie, Z. M.; Wang, W.; Viswanathan, V. V.; Lee, Y. J.; Zhang, J. G.; Graff, G. L.; Yang, Z. G.; Liu, J. LiMnPO4 nanoplate grown via solid-state reaction in molten hydrocarbon for Li-ion battery cathode. *Nano Lett.* **2010**, *10*, 2799−2805.

(52) Kim, H.; Yoon, G.; Park, I.; Park, K. Y.; Lee, B.; Kim, J.; Park, Y. U.; Jung, S. K.; Lim, H. D.; Ahn, D.; Lee, S.; Kang, K. Anomalous Jahn-Teller behavior in a manganese-based mixed-phosphate cathode for sodium ion batteries. *Energy Environ. Sci.* **2015**, *8*, 3325−3335.

(53) Kim, S. W.; Seo, D. H.; Kim, H.; Park, K. Y.; Kang, K. A comparative study on Na2MnPO4F and Li2MnPO4F for rechargeable battery cathodes. *Phys. Chem. Chem. Phys.* **2012**, *14*, 3299−3303.

(54) Aydinol, M. K.; Kohan, A. F.; Ceder, G.; Cho, K.; Joannopoulos, J. Ab initio study of lithium intercalation in metal

oxides and metal dichalcogenides. *Phys. Rev. B: Condens. Matter Mater. Phys.* **1997**, *56*, 1354−1365.

(55) Jain, A.; Ong, S. P.; Hautier, G.; Chen, W.; Richards, W. D.; Dacek, S.; Cholia, S.; Gunter, D.; Skinner, D.; Ceder, G.; Persson, K. A. Commentary: The Materials Project: A materials genome approach to accelerating materials innovation. *APL Mater.* **2013**, *1*, 011002.

(56) Chotard, J. N.; Rousse, G.; David, R.; Mentre, O.; Courty, M.; Masquelier, C. Discovery of a sodium-ordered form of Na3V2(PO4)3 below ambient temperature. *Chem. Mater.* **2015**, *27*, 5982−5987.

(57) Delmas, C.; Nadiri, A.; Soubeyroux, J. L. The nasicon-type titanium phosphates ATi2(PO4)3 (A = Li, Na) as electrode materials. *Solid State Ionics* **1988**, *28*, 419−423.

(58) d'Yvoire, F.; Pintard-Screpel, M.; Bretey, E.; de la Rochere, M. Phase transitions and ionic conduction in 3D skeleton phosphates A3M2(PO4)3: A = Li, Na, Ag, K; M = Cr, Fe. *Solid State Ionics* **1983**, *9−10*, 851−857.

(59) Cherkaoui, F.; Viala, J. C.; Delmas, C.; Hagenmuller, P. Crystal chemistry and ionic conductivity of a new Nasicon-related solid solution Na1+xZr2-x/2Mgx/2(PO4)3. *Solid State Ionics* **1986**, *21*, 333−337.

(60) Shannon, R. D.; Prewitt, C. T. Effective ionic radii in oxides and fluorides. *Acta Crystallogr., Sect. B: Struct. Crystallogr. Cryst. Chem.* **1969**, *25*, 925−946.

(61) Padhi, A. K.; Nanjundaswamy, K. S.; Goodenough, J. B. Phospho-olivines as positive-electrode materials for rechargeable lithium batteries. *J. Electrochem. Soc.* **1997**, *144*, 1188−1194.

(62) Jian, Z. L.; Yuan, C. C.; Han, W. Z.; Lu, X.; Gu, L.; Xi, X. K.; Hu, Y. S.; Li, H.; Chen, W.; Chen, D. F.; Ikuhara, Y.; Chen, L. Q. Atomic structure and kinetics of NASICON NaxV2(PO4)3 cathode for sodium-ion batteries. *Adv. Funct. Mater.* **2014**, *24*, 4265−4272.

(63) Cerrato, J. M.; Hochella, M. F.; Knocke, W. R.; Dietrich, A. M.; Cromer, T. F. Use of XPS to identify the oxidation state of mn in solid surfaces of filtration media oxide samples from drinking water treatment plants. *Environ. Sci. Technol.* **2010**, *44*, 5881−5886.

(64) Tang, W.; Sanville, E.; Henkelman, G. A grid-based Bader analysis algorithm without lattice bias. *J. Phys.: Condens. Matter* **2009**, *21*, 084204.

(65) Goodenough, J. B. Jahn-Teller phenomena in solids. *Annu. Rev. Mater. Sci.* **1998**, *28*, 1−27.

(66) Yamada, A.; Tanaka, M.; Tanaka, K.; Sekai, K. Jahn-Teller instability in spinel Li-Mn-O. *J. Power Sources* **1999**, *81*, 73−78.

(67) Piper, L. F. J.; Quackenbush, N. F.; Sallis, S.; Scanlon, D. O.; Watson, G. W.; Nam, K. W.; Yang, X. Q.; Smith, K. E.; Omenya, F.; Chernova, N. A.; Whittingham, M. S. Elucidating the nature of pseudo Jahn-Teller distortions in LixMnPO4: Combining density functional theory with soft and hard X-ray spectroscopy. *J. Phys. Chem. C* **2013**, *117*, 10383−10396.